

Adaptive Multiscale–Streamline Simulation and Inversion for High-Resolution Geomodels

Knut–Andreas Lie Vegard Røine Stenerud Atgeirr Flø Rasmussen

June 30, 2008

Abstract

First, we present an efficient method for integrating dynamic data in high-resolution subsurface models. The method consists of two key technologies: (i) a very fast multiscale–streamline flow simulator, and (ii) a fast and robust ‘generalized travel-time inversion’ method. The travel-time inversion is based on sensitivities computed analytically along streamlines using only one forward simulation. The sensitivities are also used to selectively reduce the updating of basis functions in the multiscale mixed finite-element pressure solver. Second, we discuss extensions of the methodology to grids with large differences in cell sizes and unstructured connections. To this end, we suggest to use rescaled sensitivities (average cell volume multiplied by local sensitivity density) in the inversion and propose a generalized smoothing operator for the regularization to impose smooth modification on reservoir parameters. Two numerical examples demonstrate that this reduces undesired grid effects. Finally, we show a slightly more complex example with two faults and infill drilling.

Introduction

History matching refers to the process of modifying a reservoir description to match measured dynamic reservoir responses. Typical examples of this process may be described by a loop consisting of four elements and a conditional: (i) start with a grid description of the reservoir and its media properties, (ii) perform a flow simulation using the forward reservoir model to obtain dynamic flow responses, and (iii) evaluate the misfit between the calculated and observed responses. If this misfit is sufficiently small, the loop terminates. If not, one inverts the dynamic data to a new set of media properties and returns to the first step.

Although the principles of history matching are easy to describe, it is nontrivial to find a good practical algorithmic realisation. First of all, the inverse problem associated with the data matching is generally ill-posed and does not have a unique (and stable solution). The forward model is nonlinear and may be biased, and it is often difficult to describe and quantify errors in the flow model, the data, and the numerical methods. Second, one has to choose a suitable subset of the parameters that makes it possible to match the observed data without overestimating. Most formulations lead to (highly) non-convex and oscillatory misfit functionals, and finally, the forward simulations are computationally demanding. In this paper, we present two key ideas that address the last two problems for the particular case where permeability data are matched based on observation of water-cut data.

The *generalized travel-time* (GTT) inversion method was introduced by Vasco et al. (1999) and He et al. (2002) and has been successfully applied to several field cases, see e.g., Qassab et al. (2003) and Hohl et al. (2006). By matching travel time rather than amplitudes, the misfit functional exhibits quasilinear properties (Cheng et al., 2005b) and can be attacked using a standard iterative least-squares minimization algorithm by adding appropriate regularization terms that help preserve geologic realism, keep changes to prior model minimal, and only allow smooth large-scale changes. Although the inversion method itself does not require a streamline simulator (Cheng et al., 2005a), it is most efficient if the required production-response sensitivities are approximated by analytical integrals streamlines and a streamline simulator is used for the forward simulation. In this paper, we discuss how the GTT methodology and the calculation of sensitivities can be extended to (corner-point) grids with large differences in cell sizes and unstructured grids.

To address the last question, we have previously shown (Stenerud et al., 2008, 2007a) how the GTT inversion can be combined with a multiscale-streamline solver to provide highly efficient computations of the forward model. In particular, we have shown how the sensitivities from the inversion method can be used to reduce the computational work of the multiscale flow solver in regions of low sensitivity, thereby reducing the simulation time considerably with negligible loss in accuracy compared with a conventional reservoir simulator.

Flow Model and Numerical Methods

We consider incompressible, immiscible two-phase flow of oil and water and will for simplicity neglect gravity, compressibility, and capillary forces. For simplicity, we assume constant porosity $\phi \equiv 1$ and focus only on history matching the absolute permeability $K(x)$, which is assumed to be a diagonal tensor. The forward model consists of a first-order elliptic system for the pressure p and Darcy velocity \vec{v} ,

$$\nabla \cdot \vec{v} = q_t, \quad \vec{v} = -\lambda_t(S)K\nabla p, \quad (1)$$

and a hyperbolic transport equation for the water saturation, $\partial_t S + \nabla \cdot (f_w(S)\vec{v}) = q_w$. By making a coordinate transform, this equation can be cast into a family of one-dimensional equations along streamlines using the time-of-flight, $\tau = \int \phi(r)/|\vec{v}(r)|dr$, as a spatial coordinate.

To solve the pressure equation (1), we will use a finite-volume method (two-point or a mimetic method (Aarnes et al., 2008)) or the multiscale mixed finite element method (Aarnes et al., 2004, 2008). The multiscale method solves the flow equations on a coarser grid using coarse-grid basis functions that incorporate subgrid velocity (or flux) variations from the original

fine grid. These basis functions are constructed numerically by solving a local flow problem, as in a flow-based upscaling method, but unlike an upscaling method, we keep the whole local flow solution as a building block for the global solution and not just the average in the form of an upscaled permeability or transmissibility. By using the subgrid resolution of the basis functions, we obtain an approximate solution on the fine grid at the cost of solving a global problem on the coarsened grid. The blocks in the coarse grid can be formed by accumulating almost arbitrary connected collections of cells from the fine grid, meaning that the coarse grid can easily be adapted to follow geological features and well paths. Previous studies (Aarnes et al., 2008; Kippe et al., 2008) show that the multiscale method is very robust with respect to the shape of the coarse blocks.

Solving local flow problems is typically the most expensive step in a multiscale method. All basis functions must be constructed initially and will generally be time-dependent through $\lambda(S)$. The total mobility, however, is a relatively smooth and slowly varying function away from strong saturation fronts, meaning that the basis functions need only to be recomputed infrequently. Reuse of basis functions is the key to high efficiency of multiscale methods compared with e.g., a domain-decomposition or a multigrid approach for solving the global flow problem directly on the fine grid. In a history-matching setting, where one performs multiple flow simulations on models that differ only a little, one can in addition reuse basis functions from the previous forward simulation. This means that the multiscale flow solver will be efficient when used in history matching. Herein we will use sensitivities from the inversion method to determine areas that have little effect on the production responses and in which the basis functions therefore need not be updated. If multiple realizations are simulated in parallel, one may use a common, extended set of basis functions that spans out the stochastic variability, see (Aarnes and Efendiev, 2007).

Generalized Travel-Time Inversion

Generalized travel-time (GTT) inversion can be used to match several types of data, but in the following we will only consider matching permeability based on observation of water-cut data in the production wells. To measure the misfit in water cut, we start from a standard least-squares functional that for each well sums the squared deviance between the calculated response $y^{calc}(t_j)$ and the observed response $y^{obs}(t_j)$ at each data point t_j , possibly weighted by a scalar that measures our trust in each observation. The usual approach is now to try to match the amplitude of y^{calc} to the observation y^{obs} at every data point. The GTT approach, on the other hand, assumes that the amplitude is (almost) correct, but that the time it is observed is wrong. We therefore seek a time-shift Δt in the calculated responses that minimize the sum of the squared deviance between $y^{obs}(\cdot)$ and $y^{calc}(\cdot - \Delta t)$. However, rather than using the least-squares functionals to determine the optimal time shifts for each well, we use the coefficient of determination

$$\mathcal{R}^2(\Delta t) = 1 - \frac{\sum_j (y^{obs}(t_j + \Delta t) - y^{calc}(t_j))^2}{\sum_j (y^{obs}(t_j) - \overline{y^{obs}})^2} \quad (2)$$

Once the time-shifts are determined, we need to invert them into modifications of the permeabilities. The inversion is formulated as the minimization of a regularized functional

$$\arg \min_{\delta \mathbf{K}} \|\Delta \mathbf{t} - \mathbf{G} \delta \mathbf{K}\| + \beta_1 \|\delta \mathbf{K}\| + \beta_2 \|\mathbf{L} \delta \mathbf{K}\|. \quad (3)$$

Here, the first term is the misfit and $\mathbf{G} = \{\frac{\partial \Delta t_j}{\partial K_i}\}$ the sensitivity matrix and $\delta \mathbf{K}$ is the permeability perturbation. The next two terms are regularisation terms: $\|\delta \mathbf{K}\|$ seeks to minimise the permeability modifications, and $\|\mathbf{L} \delta \mathbf{K}\|$ seeks to keep modifications as smooth as possible by introducing the smoothing operator \mathbf{L} that measures the local roughness of $\delta \mathbf{K}$. To minimize (3) one can use a standard iterative least-square algorithm.

The GTT method, as formulated above, is general and should in principle apply directly to (fully) unstructured grids. However, to obtain a practical method, with good convergence properties, we need to address some specific issues for the smoothing operator and the calculation of sensitivities.

Smoothing Operator. On Cartesian grids, L is typically a Laplacian operator, e.g., the standard five-point (2D) or seven-point (3D) stencil. How to find a good smoothing operator for fully unstructured grids is more difficult, as discussed in more detail in (Stenerud et al., 2007b). First of all, the operator should give the same smoothing effect independently of the local grid density. Second, the operator should reduce to a standard Laplacian scheme on Cartesian grids. Third, the smoothing of each cell i should depend on cells in an appropriate neighbourhood $\mathcal{N}(i)$, the influence of each neighbour j should decay by the (Euclidean) distance $\zeta(i, j)$, be zero outside some finite range, and should be bounded as the distance $\zeta(i, j)$ goes to zero. To meet these requirements, we proposed to use a stencil on the following form (centred at cell number i)

$$\begin{aligned} L_i \mathbf{m} &= -w_{ii}m_i + \sum_{j \in \mathcal{N}(i)} w_{ji}m_j, \\ w_{ji} &= w_{\text{norm}} \cdot \rho(\zeta(i, j); R), \quad w_{ii} = \sum_{j \in \mathcal{N}(i)} w_{ji}. \end{aligned} \quad (4)$$

Here, $\mathcal{N}(i)$ gives the neighbourhood; $\rho(\zeta; R, \dots)$ is a standard correlation function from geo-statistics, where the generalized correlation length R is used to control the range of influence for ρ ; and w_{norm} is a normalization weight used to ensure that the influence of each neighbourhood is approximately the same, see (Stenerud et al., 2007b) for more details.

The number of cells in a k -ring¹ neighbourhood \mathcal{N}_k is bounded by k times the number of faces (or edges) per cell independent of cell sizes, i.e., by $6k$ in a corner-point grid, except near faults where there may be more non-neighbouring connections. The number of cells in a radius² neighbourhood $\mathcal{N}_{r=R}$ varies with the grid density and we therefore expect it to be more robust and less grid-dependent.

Correlation functions are used to model the covariance structure of a random spatial quantity. Some readers may be more familiar with the variogram function $\gamma(\zeta; R)$. For a stationary Gaussian random field, the two are related as follows: $\gamma(\zeta; R) = \sigma^2(1 - \rho(\zeta; R))$, where σ^2 is the variance. In the following we will either use the constant correlation function $\rho_{\text{const}}(\zeta; R)$ that equals one for $\zeta \leq R$ and zero elsewhere, or the exponential correlation function $\rho_{\text{exp}}(\zeta; R, \nu) = \exp(-3(\zeta/R)^\nu)$, which decays with increasing distance.

Sensitivities. By using a streamline simulator for the forward model, all entries in the sensitivity matrix $G_{ij} = \frac{\partial \Delta t_j}{\partial K_i}$ can be approximated in terms of analytical integrals and be determined very efficiently from a single forward simulation. First, observe that water-cut curves are calculated by averaging the fractional flow at the outlet of all streamlines connected to a producer. The only effect of a permeability perturbation δK_i in cell i , is to perturb the time-of-flight of all streamlines passing through that cell, thereby delaying or speeding up the arrival of a certain saturation value at the streamline outlet. This will, in turn, introduce a time shift in the overall water cut at the well. Now, let τ_ℓ denote the time-of-flight at the outlet of streamline Ψ_ℓ . Then,

$$\frac{\partial \tau_\ell}{\partial K_i} = \frac{\partial \Delta \tau_{\ell,i}}{\partial K_i} = \int_{\Delta \Psi_{\ell,i}} \frac{\partial s(\xi)}{\partial K_i} d\xi = - \int_{\Delta \Psi_{\ell,i}} \frac{s(\xi)}{K_i} d\xi = - \frac{\Delta \tau_{\ell,i}}{K_i}, \quad (5)$$

where $\Delta \tau_{\ell,i}$ is the time-of-flight of the streamline increment $\Delta \Psi_{\ell,i}$ through cell i and $s(\xi)$ is the 'slowness' function $\phi(\xi)/|\vec{v}(\xi)|$. To relate the perturbation of τ to the shift in the water-cut

¹The k -ring (or k th order) neighbourhood includes all cells that can be reached by k edges or less in the connectivity graph in which the centroids of each cell is a vertex.

²The radius neighbourhood with radius r includes all cells that can be reached by a search in the connectivity graph without violating $\zeta(i, j) \leq r$. The radius neighbourhood should at least include the 1-ring neighbour.

curve, we make the approximation that the saturation along each streamline follows a Buckley–Leverett profile. At the outlet, $f'_c(S_{o,\ell}) = \tau_\ell/t_j$, where f_c is the convex hull of the fractional-flow function and $S_{o,\ell}$ is the outlet saturation. In the GTT method, we assume that $S_{o,\ell}$ is fixed. Hence, $\partial t_j/\partial K_i$ is proportional to $\partial \tau_\ell/\partial K_i$. The sensitivity of Δt follows by summing over all streamlines and using the definition that $N\Delta t = -\sum_j t_j$ for N observation points.

It follows from the above formulation that the sensitivities are additive. For a general polyhedral cell, one can therefore find the sensitivity by subdividing the cell into simplexes, on which sensitivities are easily determined. However, this will not be necessary for hexahedral cells in corner-point grids, for which efficient streamline tracing methods exist.

Because sensitivities are additive, they scale with the volume of the cell, which implies that too small/large modifications may be imposed on small/large cells during the history match. To exemplify, let us imagine that we split one of the cells in two. Because the sensitivity in the new cells is one half of the sensitivity in the unsplit cell, the permeability modification in the two half-cells will be smaller than if they were considered as one (unsplit) cell. Accordingly, it is natural to use scaled sensitivities adjusted for cell volume (i.e., the sensitivity density in each cell multiplied by the average cell volume) to remedy this undesired grid effect for cases with large variations in cell sizes. Scaling sensitivities will make it more difficult to match data, but will generally improve the predictive power of the derived permeability fields.

Numerical Examples

The versatility of the generalized travel-time inversion algorithm has been extensively discussed in publications by Datta–Gupta and coworkers, see e.g., (Vasco et al., 1999; He et al., 2002; Qassab et al., 2003; Hohl et al., 2006). Similarly, the potential speedup that can be obtained from using a multiscale pressure solver is thoroughly discussed by Stenerud et al. (2008, 2007a). Herein, we will therefore focus on a few special issues that arise when applying the GTT methodology to unstructured grids. To keep the presentation simple, we will present two synthetic and idealized cases to illustrate properties of the sensitivities and the smoothing operators that one should keep in mind when applying the technology to unstructured grids or grids with large differences in cell sizes. Finally, we present a more complex case with two faults and infill drilling.

For all cases considered, the flow is described using quadratic relative permeability curves with individually specified end-point mobility ratios. For simplicity, the examples use a standard pressure solver: for greater computational efficiency, a multiscale solver could have been used.

Example 1: *To illustrate the effect arising from (large) difference in cell sizes, we consider an unstructured triangular grid with 581 cells inside a bounding box of 322×318 meters, containing a ring with high cell density, see Figure 1. The contrived reservoir is produced using an inverted nine-spot. Synthetic data from 1200 days of production are obtained by adding 5% (white) noise to the results of a streamline simulation using a mixed finite-element pressure solver. In the inversion, we use data from the first 800 days. The remaining 400 days are used to assess the predictive ability of our method. The initial model is assumed to be homogeneous with 7 mD.*

Table 1 reports time-shift and amplitude residuals for four different smoothing operators and Figure 1 shows the resulting permeability fields after eight iterations. All operators capture the large-scale trends. Because there is no initial heterogeneity to preserve, the matched fields are too smooth, in particular for operators #3 and #4. The residuals are lowest for operators #1 and #2. On the other hand, the smoothing in these operators does not extend across the ring of small cells. Hence, too small modifications are imposed inside the ring unless one uses rescaled densities. For operators #3 and #4, the influence region for each cell is larger, and modifications induced by large sensitivities nearby are distributed into the ring with small cells. We also observe that whereas $\Delta \ln K$ decreases, the residuals increase when we introduce the rescaled sensitivities. This is a result of the fact that matching becomes more difficult, because

Table 1: Time-shift (T) and amplitude (A) residual measured in percentage of initial and reduction in permeability discrepancy ($\Delta \ln K = \|\ln K_{\text{true}} - \ln K_{\text{match}}\|$) with four different smoothing operators and original and scaled sensitivities.

	Operators		Unscaled			Scaled		
	Nbh	ρ	T	A	$\Delta \ln K$	T	A	$\Delta \ln K$
Initial	—	—	100.0	100.0	1.165	100.0	100.0	1.165
Op #1	\mathcal{N}_1	$\rho_{\text{const}}(\cdot; 5)$	6.0	14.2	0.771	7.0	16.1	0.631
Op #2	\mathcal{N}_2	$\rho_{\text{const}}(\cdot; 5)$	8.2	18.9	0.612	12.6	22.5	0.525
Op #3	$\mathcal{N}_{r=30}$	$\rho_{\text{exp}}(\cdot; 5, 2)$	9.5	18.6	0.585	12.1	20.8	0.546
Op #4	$\mathcal{N}_{r=40}$	$\rho_{\text{exp}}(\cdot; 5, 2)$	12.0	20.9	0.555	12.4	21.7	0.568

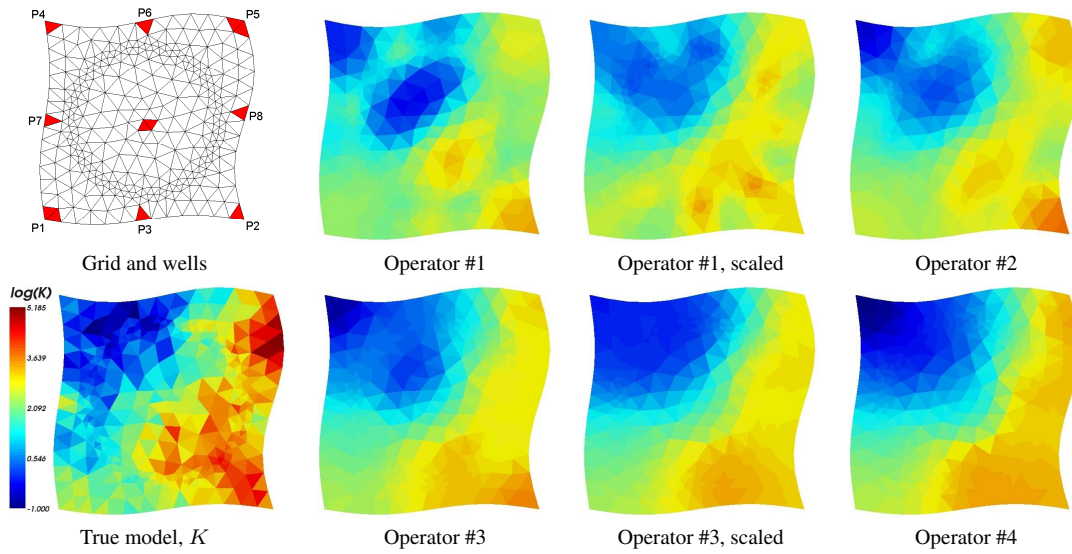


Figure 1: Grid and well configuration, reference permeability field, and derived permeability fields for operators #1 to #4, see Table 1.

rescaled sensitivities will enforce greater modifications in cells that are less important to shifting the production curves.

Figure 2 shows a comparison of the initial and final match of the water-cuts obtained by operator #4 with unscaled sensitivities for three selected wells: the well with best match (P8), the well with worst match (P2), and the well with least data (P4). For all wells, the match and the prediction are satisfactory, and in particular for well P4, which had almost no production history during the data period.

The example above demonstrated that grid effects arising due to differences in cell sizes can be counteracted by using a radius neighborhood rather than a k -ring neighbourhood in the smoothing operator, or alternatively by using scaled sensitivities. For layered reservoirs, smoothing across geological layers is undesirable if one is to preserve the layered structure. A natural strategy is therefore to use smoothing operators with significantly larger neighbourhood and/or correlation lengths in the horizontal than in the vertical direction.

Example 2: In the next example, we demonstrate grid effects arising in models containing thin geological layers. To this end, we consider a simple $21 \times 21 \times 7$ tensor-product grid with homogeneous permeability and where the relative thickness of the horizontal grid layers varies throughout the model, as shown in Figure 3. The homogeneous permeability is chosen on purpose to accentuate the undesired grid effects. However, we remark that such a structure may arise in sublayers within the stratigraphic column in high-resolution geomodels or for models with local grid refinement.

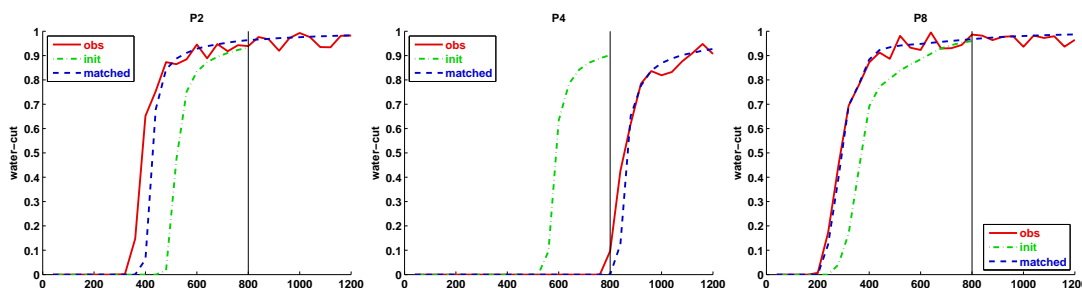


Figure 2: Water-cut match for operator #4 for wells P2, P4, and P8. The first 800 days constitute the matching period, while the next 400 days are predicted.

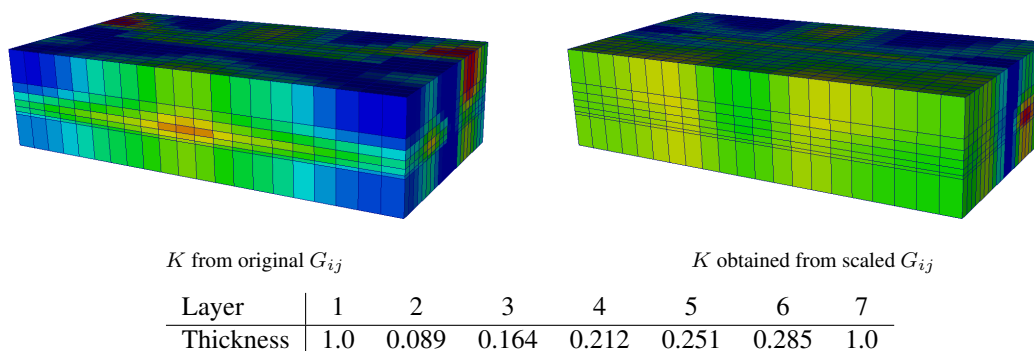


Figure 3: History matched permeability for a homogeneous reservoir with varying vertical thickness of grid layers. The initial model has too high permeability in the front half and too low permeability in the back half.

The reservoir is produced through an inverted nine-spot well pattern, with an injector in the middle and producers in the four corners and at the center of each vertical side. We match synthetic water-cut data obtained from a flow simulation using a sequentially implicit finite-volume solver, which generally smears the solution compared with the streamline solver. Figure 3 shows matched permeability fields using a prior model that assumes that the reservoir consists of two facies, one with too high permeability in the front half, and one with too low permeability in the back half. The permeability field matched using sensitivities shows large variations. In the front half, we see that almost no modifications have been imposed in the thin layers, whereas too large modifications towards lower values are imposed in the upper and lower layers to compensate for fast flow in the thin layers. With the scaled sensitivities, the variations in the front half are significantly smaller and the permeability is almost constant in each vertical column in the grid.

Example 3: Our third, and final, example considers a 50×50 corner-point grid two non-sealing strike-slip faults that introduce non-neighbouring connections, see Figure 4. Whereas the grid has three shifted sections inside a bounding box of 646×605 meters, the lognormal permeability field has a logical structure with diagonal permeability streaks. Initially, we produce the reservoir from an inverted five-spot configuration, with an injector in the center and four producers in the corners operating at equal constant rate. Producer P4 in the south-west corner has early breakthrough and is converted to an injector after 900 day. After conversion, P4 has 3/5 of the total injection rate. Simultaneously, a new producer (P5) is added in the south-west corner of the middle section. Altogether, 2500 days of synthetic production data are obtained by adding 15% white noise to a streamline simulation of the reference model.

As our prior model, we use another realization from the same heterogeneity model, conditioned on the true permeabilities in the well blocks. Table 2 reports reduction in time-shift

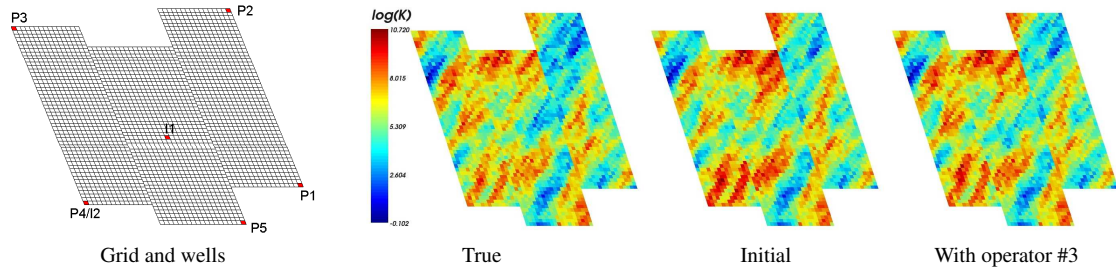


Figure 4: Grid and well configuration and permeability fields for Example 3.

Table 2: Time-shift (T) and amplitude (A) residual measured in percentage of initial and reduction in permeability discrepancy ($\Delta \ln K = \|\ln K_{\text{true}} - \ln K_{\text{match}}\|$) with four different smoothing operators.

	Nbh	ρ	T	A	$\Delta \ln K$
Initial	—	—	100.0	100.0	0.421
Op #1	\mathcal{N}_1	$\rho_{\text{const}}(\cdot; 5)$	5.5	35.0	0.334
Op #2	\mathcal{N}_2	$\rho_{\text{const}}(\cdot; 5)$	4.9	35.0	0.332
Op #3	$\mathcal{N}_{r=30}$	$\rho_{\text{exp}}(\cdot; 5, 2)$	5.8	35.2	0.334
Op #4	$\mathcal{N}_{r=40}$	$\rho_{\text{exp}}(\cdot; 5, 2)$	5.7	35.8	0.332

and amplitude residuals and permeability discrepancy derived with four different smoothing operators. Figure 4 shows the derived match for operator #3 along with the true and the initial permeability. From the figure we clearly see that the inversion preserves geological realism from the prior model without introducing any smearing across the faults. The match of the water-cut data are shown in Figure 5. Overall, the match to the production data and the quality of the derived permeability fields are satisfactory.

Concluding Remarks

Multiscale-streamline inversion is a promising methodology for history-matching highly detailed reservoir models with a large number of cells. Admittedly, the methodology has a large number of parameters and effects: regularization parameters, scaled or unscaled sensitivities, smoothing operator with accompanying parameters (neighbourhood, correlation, and normalization weights), number of streamlines in forward simulation and for calculating sensitivities, and choice of coarse grid and strategy for reusing basis functions in the multiscale solver. Fortunately, the overall methodology is relatively robust (or insensitive) with respect to the most of these parameters. However, for grids with large differences in cell sizes, we have demonstrated that better results are obtained if one uses sensitivities scaled by the cell volume rather than the original time-shift sensitivities. Similarly, for unstructured grids, some care should be taken in choosing the smoothing operators.

References

- Aarnes, J.E. and Efendiev, Y. [2007] Mixed multiscale finite element for stochastic porous media flows. *SIAM J. Sci. Comp.*, submitted.
- Aarnes, J.E., Kippe, V., and Lie, K.A. [2004] Mixed multiscale finite elements and streamline methods for reservoir simulation of large geomodels. *Adv. Water Resour.*, **2**(3), 421–439.
- Aarnes, J.E., Krogstad, S., and Lie, K.A. [2008] Multiscale mixed/mimetic methods on corner-point grids. *Comput. Geosci.* Doi: 10.1007/s10596-007-9072-8.
- Cheng, H., Kharghoria, A., He, Z., and Datta-Gupta, A. [2005a] Fast history matching of finite-difference models using streamline-derived sensitivities. *SPE Reserv. Eval. Eng.*, **8**(5), 426–436.

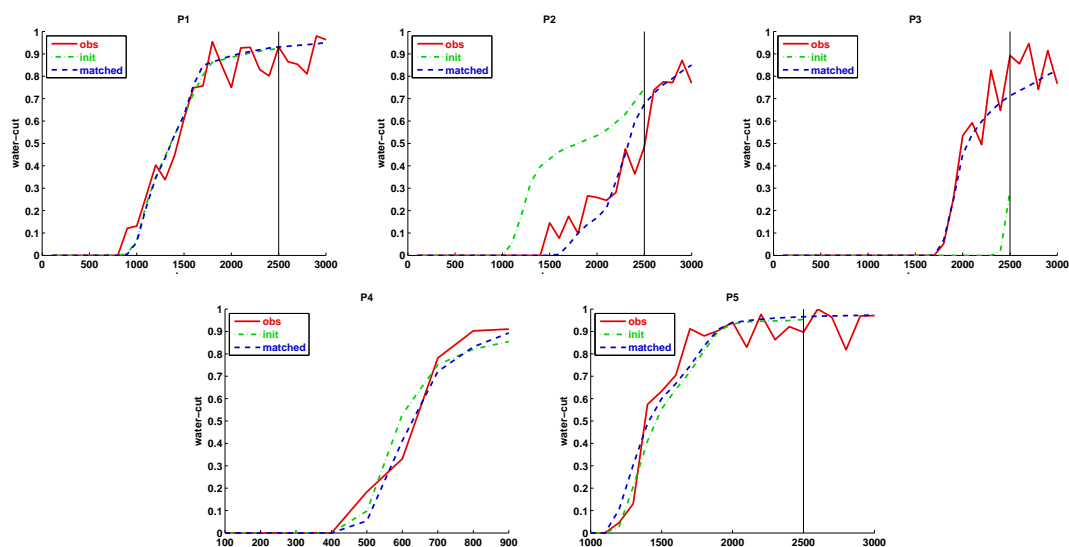


Figure 5: Water-cut match for operator #3 for Example 3. The first 2500 days are used to match data, where as the last 500 days is for prediction

Cheng, H., Datta-Gupta, A., and He, Z. [2005b] A comparison of travel-time and amplitude matching for field-scale production-data integration: Sensitivity, nonlinearity, and practical implications. *SPE J.*, **10**(1), 75–90.

He, Z., Yoon, S., and Datta-Gupta, A. [2002] Streamline-based production data integration with gravity and changing field conditions. *SPE J.*, **7**(4), 423–436.

Hohl, D., Jimenez, E.A., and Datta-Gupta, A. [2006] Field experiences with history matching an offshore turbiditic reservoir using inverse modeling. In: *SPE Annual Technical Conference and Exhibition*. San Antonio, TX, USA. SPE 101983.

Kippe, V., Aarnes, J.E., and Lie, K.A. [2008] A comparison of multiscale methods for elliptic problems in porous media flow. *Comput. Geosci.* Doi: 10.1007/s10596-007-9074-6.

Qassab, H., R, M.K., Pavlas, Afaleg, N., Ali, H., Kharghoria, A., He, Z., Lee, S.H., and Datta-Gupta, A. [2003] Streamline-based production data integration under realistic field conditions: Experience in a giant Middle-Eastern reservoir. In: *SPE Annual Technical Conference and Exhibition*. Denver, Colorado, USA. SPE 84079.

Stenerud, V.R., Kippe, V., Lie, K.A., and Datta-Gupta, A. [2007a] Multiscale-streamline simulation and dynamic data integration for high-resolution subsurface models. *submitted*.

Stenerud, V.R., Kippe, V., Lie, K.A., and Datta-Gupta, A. [2008] Adaptive multiscale streamline simulation and inversion for high-resolution geomodels. *SPE J.*, **13**(1), 99–111.

Stenerud, V.R., Lie, K.A., and Kippe, V. [2007b] Generalized travel-time inversion on unstructured grids. *submitted*.

Vasco, D., Yoon, S., and Datta-Gupta, A. [1999] Integrating dynamic data into high-resolution models using streamline-based analytic sensitivity coefficients. *SPE J.*, **4**(4), 389–399.